Hindawi
Advances in Materials Science and Engineering
Volume 2018, Article ID 5464295, 21 pages
https://doi.org/10.1155/2018/5464295

Research Article

Numerical Simulation of Rock Plate Cutting with Three Sides Fixed and One Side Free

Zhenguo Lu, Lirong Wan, Qingliang Zeng, Xin Zhang, and Kuidong Gao

College of Mechanical and Electronic Engineering, Shandong University of Science and Technology, Qingdao 266590, China

Correspondence should be addressed to Qingliang Zeng; qlzeng@sdust.edu.cn

Received 30 October 2017; Revised 15 January 2018; Accepted 6 February 2018; Published 25 June 2018

Academic Editor: Antonio Riveiro

In order to overcome conical pick wear in the traditional rock cutting method, a new cutting method was proposed on account of increasing free surface of the rock. The mechanical model of rock plate bending under concentrated force was established, and the first fracture position was given. The comparison between experimental and numerical results indicated that the numerical method is effective. A computer code LS-DYNA (3D) was employed to study the cutting performance of a conical pick. To study the rock size influenced on the cutting performance, the numerical simulations with different thickness, width, and height of a rock plate was carried out. The numerical simulation with the different cutting parameters of cutting speed, cutting angle, and cutting position influenced on cutting performance was also carried out. The numerical results indicated that the peak force increased with the increasing thickness of rock plate. With the increasing width and height of the rock plate, the peak force decreased and then became stable. Besides, the peak force decreased with the increasing of cutting position l_{xp}/l_x. Moreover, the peak force increased and then decreased with the increasing of cutting angle. The cutting speed has nonsignificant influence on the peak force. The strong exponential relationship was obtained between the peak force and cutting position, thickness, height, and width of the rock plate at a confidence level of 0.95. A binomial relationship was observed between the peak force and cutting angel. The cutting force comparison between traditional rock cutting and rock plate cutting indicated that the new cutting method can effectively reduce peak cutting force.

1. Introduction

Rock cutting is frequently encountered in some industry, for example, tunnel excavation, coal and rock mining, oil exploitation, and metal mining. As a typical excavation machine for rock cutting, a roadheader is widely used in underground tunneling engineering. For a given rock formation, the cutting method and the peak cutting forces during rock cutting process are very important for researchers to design the roadheaders and cutting tools.

Many scholars have made several attempts to research the rock fracture mechanism and predict cutting forces using theoretical, experimental, and numerical approaches. The pioneering work on conical pick cutting theories was performed by Evans [1–3]. Evans proposed that the interaction between conical pick and coal was essentially three-dimensional and concluded that the tensile and compressive strength were the primary factors influenced on mean peak cutting force in the rock cutting progress. Goktan [4] and Roxborough et al. [5] put forward revisions on Evans' cutting theory. These theories are more accurate and scientific to predict the cutting forces. With the high tensile strength rock, shear failure is the dominant property during the cutting progress [6]. Bilgin et al. [7] and Kel et al. [8] carried out the experimental researches with the linear cutting machine, in order to study the dominant rock properties that influenced on conical pick performance. Liu et al. [9] proposed a new rock cutting method and carried out the experiment to study the cutting performance. The numerical simulations are more detailed and faster than the experimental research. Huang et al. [10], Li et al. [11, 12], and Jiang et al. [13] used the finite element method (3D) in three dimensions to model rock cutting progress. They pointed out that there are close correlation between experimental and theoretical researches. Huang et al. [14] and Lei and Kaitkay [15] used PFC (2D) to simulate the rock cutting process in two dimensions, and the failure mode and hydrostatic pressure were created to research the rock failure performance.

(a) (b)

Figure 1: Conical pick wear: (a) edge wear and (b) pick head stripped.

Although considerable researches have been carried out on the classical rock cutting method, there was seldom consideration for a new cutting method. The conical picks are damaged rapidly when encounter hard rock due to the inability of conical pick and the stiffness of the cutting head. In this paper, a new rock cutting method was proposed, and new type equipment was shown. The availability of the numerical simulation was verified by theoretical analysis and experimental research. In the simulations, a damage material and the erosion criteria were used in the code to dominant the rock failure. The influence of height, thickness, and width of rock plates on crack extends, and peak force was discussed. The cutting parameters of cutting speed, cutting angle, and cutting position of the conical pick influenced on cutting performance were also discussed.

2. Proposal of the New Rock Cutting Method

Increasing the cutting power is an effective method for improving the cutting ability of the tunneling machine for cutting hard rock [16]. But on the contrary, the cutting tool wear would aggravate with the increase of cutting power as shown in Figure 1(a). Furthermore, the pick head have a great possibility to be stripped away from the conical pick as shown in Figure 1(b). Therefore, it is necessary to propose a new cutting method for cutting the hard rock.

In order to reduce the cutting force and solve the problem of conical pick wear, the diamond saw-conical pick sequential cutting method was proposed. Diamond is the hardest substance in nature, and diamond saw blades are widely used in stone exploitation and processing industry. Especially in hard rock cutting, it can obtain a good cutting performance on the basis of negligible wastage. The diamond saw was employed to slot the base rock and obtain the saw kerf as shown in Figure 2(a). The freed surfaces of the base rock increased with increasing saw kerfs and the rock plates formed. On this basis, conical picks were applied to cut the rock plates as shown in Figure 2(b). The cutting force and the wear of the conical pick could decrease significantly. Based on the

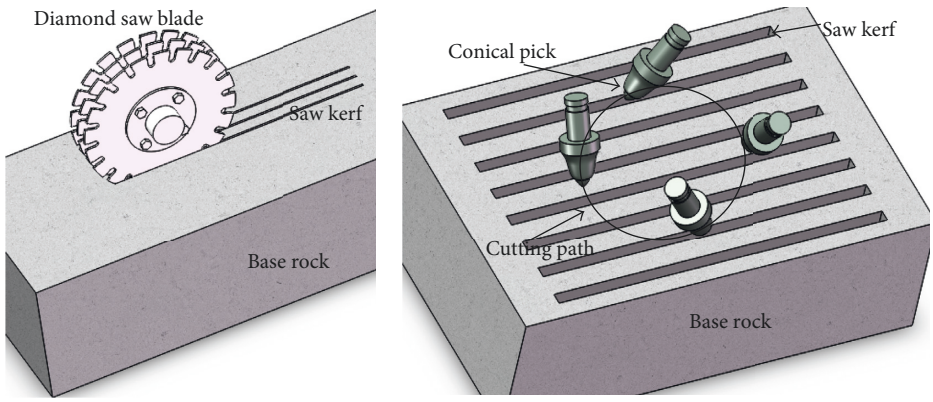

(a) (b)

Figure 2: Diamond saw-conical pick cutting method: (a) the formation of kerf and (b) rock plates cutting by conical picks.

Figure 3: Saw-pick-combined cutting machine.

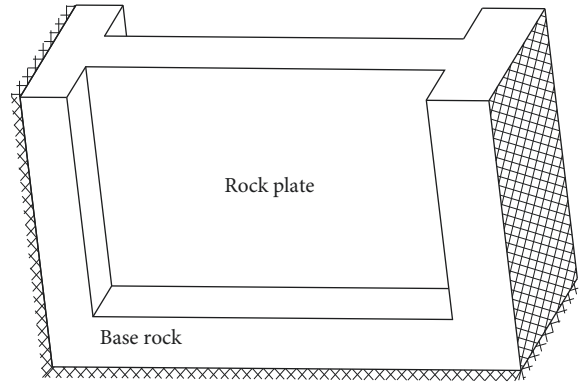

Figure 4: Three edges clamped rock plate.

new rock cutting method, the saw-pick combined cutting machinery was produced as shown in Figure 3. The interaction between conical pick and rock has a considerable value to research.

The rock plate was approximated as rectangular plates because it was narrow and long so that the radian can be ignored. The constraint conditions of rectangular rock plates depend on the base rock constraint conditions, and the three sides fixed rock plate formed as shown in Figure 4.

3. Theoretical, Experimental, and Numerical Studies

3.1. Theoretical Studies. Based on the reciprocal theorem [17, 18], the work of the first force group on the displacement corresponding to the second force group equals to the work of second force group on the displacement corresponding to the first force group. The rock plate with four edges simply supported is a basic mechanical system as shown in Figure 5(a), and the rock with the arbitrary boundary condition as the actual mechanical system is shown in Figure 5(b).

The basic mechanical system and actual mechanical system have the relationship as shown in the following equation:

$$\begin{aligned}\omega_2(\xi,\eta) &- \int_0^b V_{1,x=0}\omega_{2,x=0}\,dy + \int_0^b V_{1,x=a}\omega_{2,x=a}\,dy - \int_0^a V_{1,y=0}\omega_{2,y=0}\,dx \\ &+ \int_0^a V_{1,y=b}\omega_{2,y=b}\,dx - R_{1,00}k_1 + R_{1,a0}k_2 - R_{1,ab}k_3 + R_{1,0b}k_4 \\ &= P\omega_1(\xi,\eta) + \int_0^b M_{x=0}\omega_{1,x=0}\,dy - \int_0^b M_{x=a}\omega_{1,x=a}\,dy + \int_0^a M_{y=0}\omega_{1,y=0}\,dx - \int_0^a M_{y=b}\omega_{1,y=b}\,dx,\end{aligned} \tag{1}$$

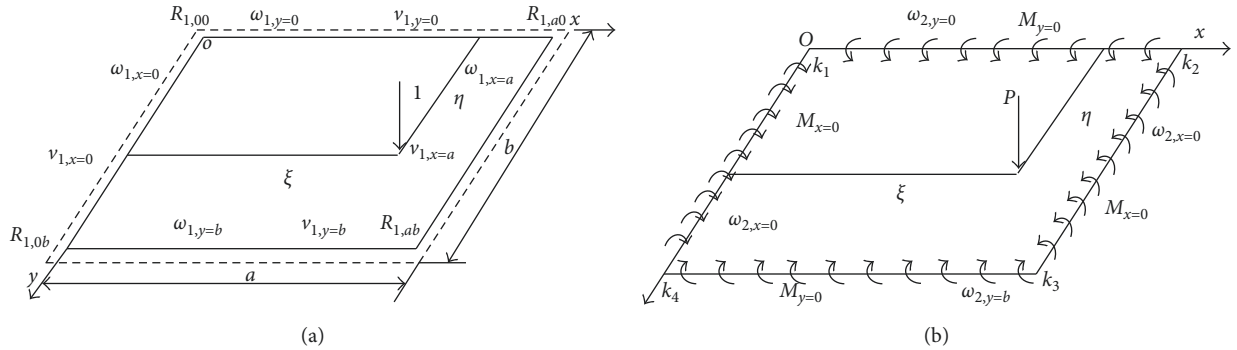

Figure 5: Solving system of bending rock plate: (a) the basic system and (b) the actual system.

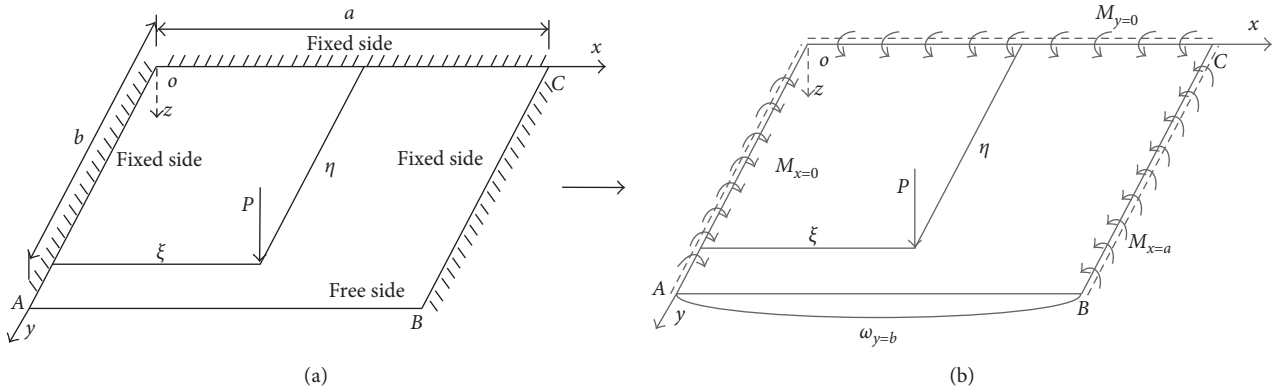

Figure 6: Mechanical model of the rock plate with three sides clamped and one side free: (a) actual system and (b) equal system.

where $\omega_1(\xi,\eta)$ is the deflection of the basic system, $\omega_2(\xi,\eta)$ is the deflection of the actual system, V is the boundary shear force, R is the angular corner force, k is the corner replacement, M is the bending moment, and P is the concentrated force. What needs to be stressed is that all the parameters in the basic system can be expressed by trigonometric series and they are known [17, 18]. The parameters are related to v (Poisson's ratio), E (modulus of elasticity), h (thickness of the rock plate), and a and b.

The rock plate with three sides fixed and one side free is shown in Figure 6(a). In order to solve the deflection of the rock plate, the fixed boundary was decomposed into the combination of simply support and bending moment as shown in Figure 6(b). Reciprocal theorem was applied between Figure 6(b) and Figure 5(a).

$$\begin{aligned}\omega_2(\xi,\eta) = P\omega_1(x_0,y_0) - \int_0^a V_{1,y=b}\omega_{2,y=b}\,dx \\ + \int_0^b M_{x=0}\omega_{1,x=0}\,dx - \int_0^b M_{x=a}\omega_{1,x=a}\,dx \\ + \int_0^a M_{y=0}\omega_{1,y=0}\,dx.\end{aligned} \tag{2}$$

where $M_{x=0}$, $M_{x=a}$, $M_{y=0}$, and $\omega_{y=b}$ can be represented by trigonometric series:

$$\begin{aligned}M_{x=0} &= \sum_{n=1,2}^{\infty} A_n \sin\beta_n y, \\ M_{x=a} &= \sum_{n=1,2}^{\infty} B_n \sin\beta_n y, \\ M_{y=0} &= \sum_{m=1,2}^{\infty} C_m \sin\alpha_m y, \\ \omega_{2,y=b} &= \sum_{m=1,2}^{\infty} D_m \sin\alpha_m y,\end{aligned} \tag{3}$$

where $\alpha m = m\pi/a$, $\beta n = n\pi/b$, and A_n, B_n, C_m, and D_m are unknown quantities in (3). The boundary condition should satisfy the following equations:

$$\begin{aligned}\left(\frac{\partial\omega_2}{\partial\xi}\right)_{\xi=0} &= 0, \\ \left(\frac{\partial\omega_2}{\partial\xi}\right)_{\xi=a} &= 0, \\ \left(\frac{\partial\omega_2}{\partial\eta}\right)_{\eta=b} &= 0, \\ \left(V_{1,\eta}\right)_{\eta=b} &= 0.\end{aligned} \tag{4}$$

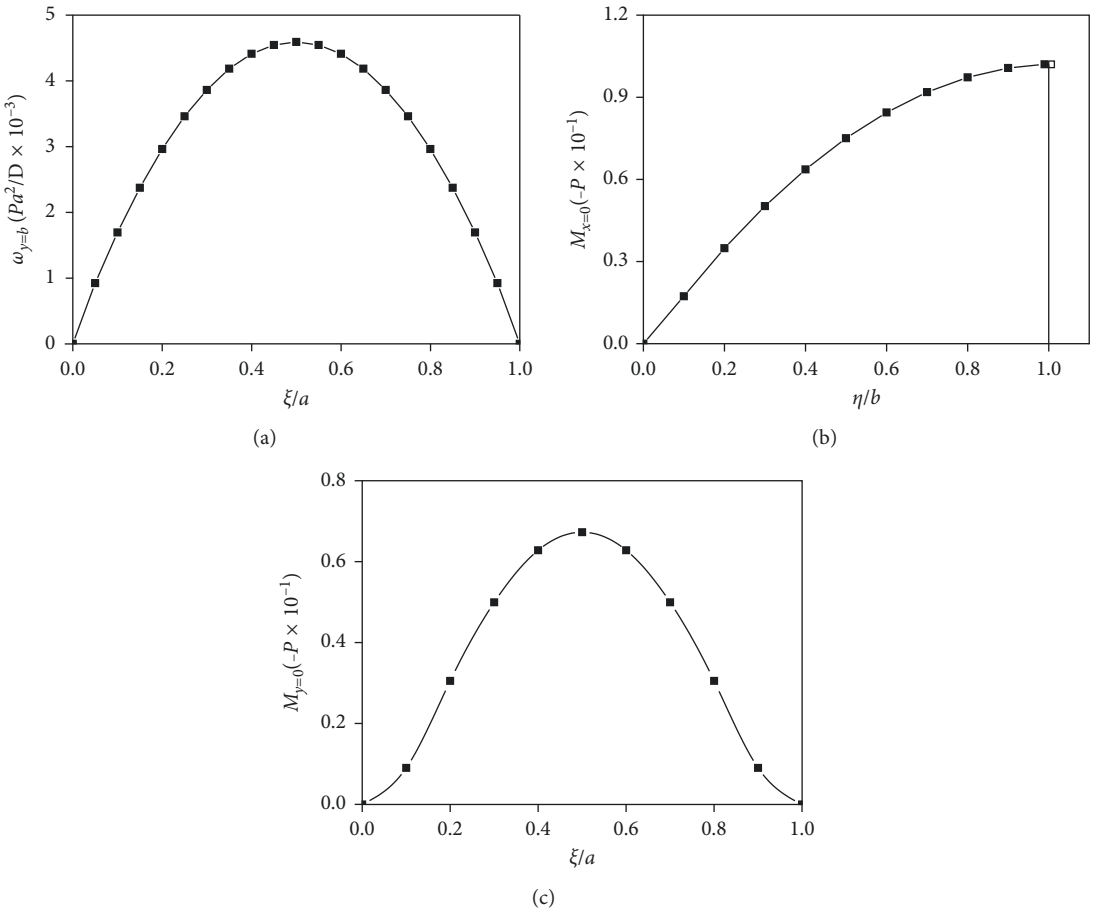

Figure 7: The solution of rock plate bending: (a) the deflection of free side, (b) bending moment as the fixed side $x = 0$, and (c) bending moment as the fixed side $y = 0$.

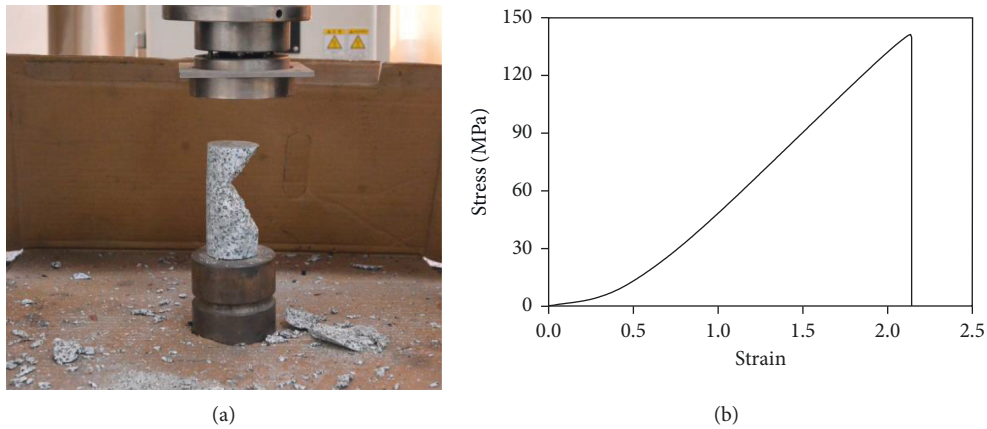

Figure 8: The experiment of granite: (a) the compression test and (b) stress-strain curve.

Table 1: Mechanical properties of the granite.

Rock name	UCS (MPa)	BTS (MPa)	E (GPa)	γ (kg/m^3)
Granite	141.3	11.5	66.2	2732

A_n, B_n, C_m, and D_m can be calculated by the combination of (2)–(4).

In order to give the solution of the rock plate bending, $a = b$, $h/a = 0.1$, and $v = 0.3$ were taken. The concentrated force was acted on ($a/2$, b). The deflection of free side is shown in Figure 7(a), where D is the bending strength. The bending moments of $M_{x=0}$ and $M_{y=0}$ are shown in Figures 7(b) and 7(c).

The maximum deflection of the free side was 4.6 ($Pa^2/D\times10^{-3}$), obtained from the middle of the free surface.

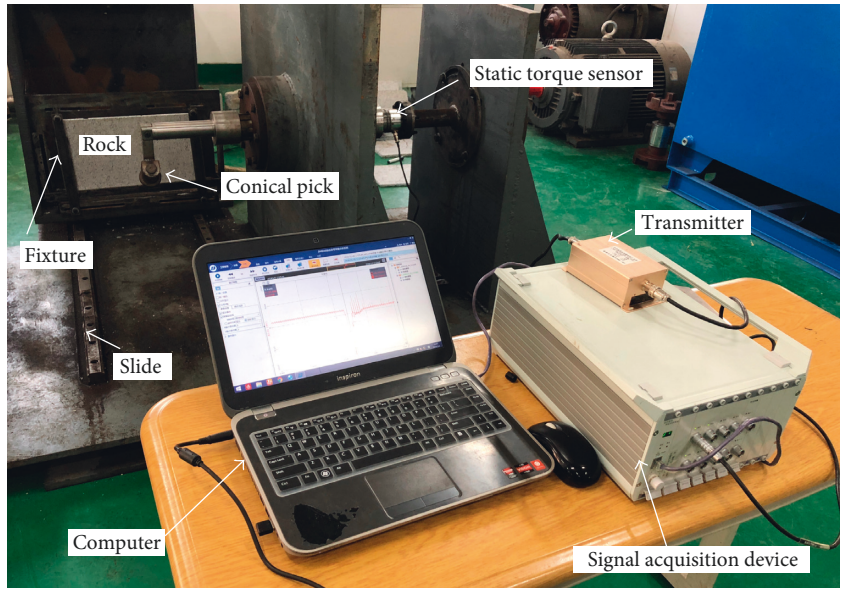

Figure 9: The rock plate cutting test bed.

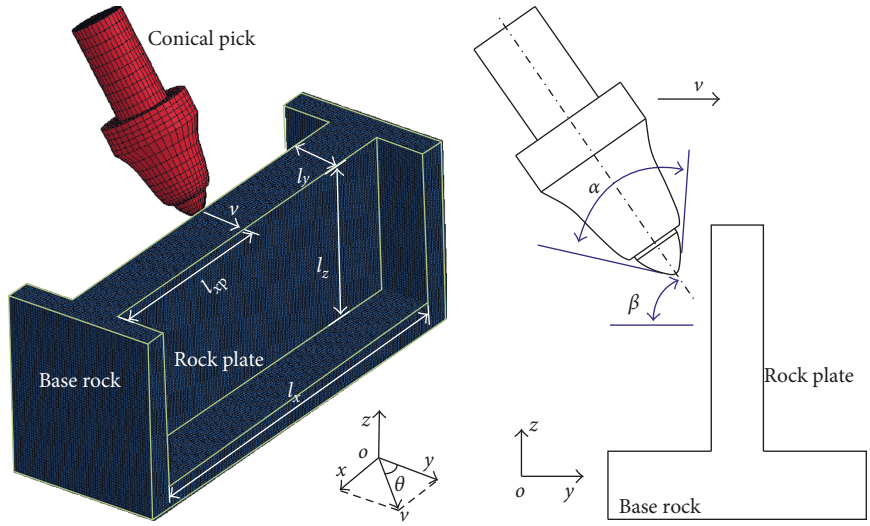

Figure 10: Rock cutting model of the rock plate: (a) rock plate cutting and (b) cutting parameters.

The maximum bending moment on the fixed side was 1.02 ($-P \times 10^{-1}$), obtained from the border of free side and fixed side. With the side $y = 0$, the maximum bending moment of 0.67 ($-P \times 10^{-1}$) was obtained. The deflection and bending moment can cause the stress of the rock plate, and the bigger the bending moment, the bigger the tensile stress [19]. Therefore, the rock plate first breaks at the junctional point of free side and fixed side, the middle of the free side, and the middle of fixed side $y = 0$.

3.2. Rock Plate Cutting Test. Mechanical properties of the rock are essential for rock plate cutting and numerical simulation. Uniaxial compression tests for uniaxial compressive strength (UCS) were carried out on a standard core sample: the cylinder which has a diameter of 50 mm and length of 100 mm. Axial loading rate was limited to 0.5~1.0 MPa/s. Axial displacement velocity is 0.1 mm/min. The Brazilian tensile strength (BTS) test was conducted on the core sample with a diameter of 50 mm and length of 50 mm. Elasticity modulus (E) was measured at 1/2 of the rock ultimate uniaxial compressive strength. In order to obtain accurate measurements, three group experiments were carried out. The density of the rock was obtained from the ratio of sample mass to sample volume. The crushed sample and the stress-strain curve are shown in Figures 8(a) and 8(b). The measurements of the granite are shown in Table 1.

The rock cutting test bed schematic in the experiments is shown in Figure 9. The static torque sensor can monitor the torque ranging from −3,000 N·m to 3,000 N·m. The transmitter output voltage ranges from −2.5 V to 2.5 V. The signal acquisition device includes ten independent input channels

Table 2: Parameters of JHC for granite.

R_o (kg·m^{-3})	G (Pa)	A	B	C	N	F_c' (Pa)	T (Pa)	$\dot{\varepsilon}_0$	ε
2732	66.2	0.79	1.6	0.007	0.61	141.3	11.5	$1e^{-6}$	0.01
$\sigma_{f,max}$	P_c (Pa)	μ_c	P_{lock} (Pa)	μ_{lock}	D_1	D_2	K_1	K_2	K_3
7	47.1	0.01	$8e^8$	0.1	0.04	1.0	$12e^9$	$25e^9$	$42e^9$

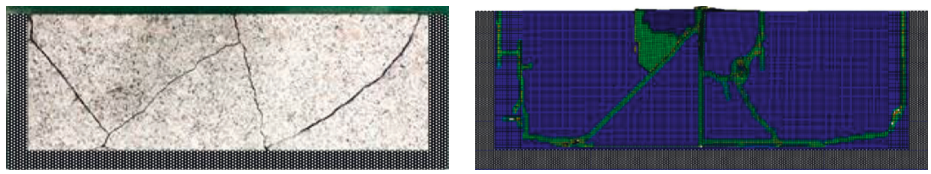

(a) (b)

Figure 11: Rock cutting results: (a) experimental results and (b) numerical results.

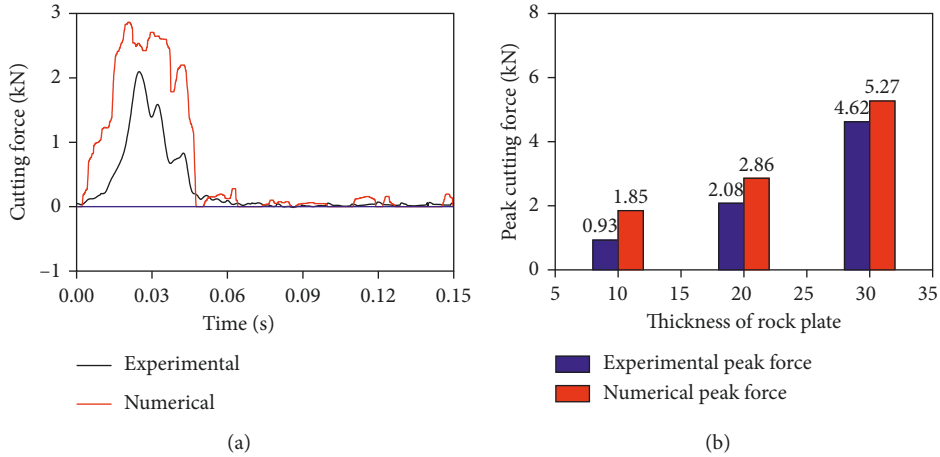

(a) (b)

Figure 12: The comparison between experimental cutting force and numerical cutting force: (a) the variation of cutting force and (b) peak cutting force.

Table 3: Mechanical properties of the base rock [8].

Properties	Compressive strength (MPa)	Tensile strength (MPa)	Elastic modulus (GPa)	Density (kg/m^3)
Sandstone 1	173.7	11.6	28	2670
Sandstone 2	113.6	6.6	17.0	2650
Sandstone 3	87.4	8.3	33.3	2670
Limestone	121.0	7.8	57	2720

and monitors the voltage data. Data sampling frequency is 10,000 HZ. A computer is used to control the acquisition device and record data. The conical pick is stable and the fixture moved linearly on the slide. In order to agree with the real rock plate cutting, three sides of the rock plate were fixed by fixture.

3.3. Numerical Model. The FEM software LS-DYNA (3D) was employed for all simulations. A conical pick and a rock were considered for modeling as shown in Figure 10(a). The material type MAT_111_JOHNSON_HOLMQUIST_CONCRETE (JHC) was given to the rock [20, 21]. The parameters of granite rock are given in Table 2. The rock consisted of two parts: base rock and rock plate. The impact angle and the tip angle of conical pick were 57° and 80°, respectively. α and β in Figure 10(b) are the tip angle and impact angle, respectively. Furthermore, the friction angle between the cutting pick and rock plates was assigned as 8.5° [7, 22]. In order to obtain crack propagation and fragment separation in the numerical simulation, a damage material model and erosion criteria were used for the base rock. The ERODING_SURFACE_TO_SURFACE and AUTOMATIC_GENERAL contact type was applied between the moved cutting pick and the stationary base rock. Hourglass and element distortion frequently occurred in the rock plate cutting progress. These situations influenced the cutting force significantly. Therefore, the fully integrated calculation method was adopted. In Figure 10(a), l_{xp} was used to express the position of the conical pick, and l_z, l_y, and l_x were height, thickness, and width of the rock plates, respectively. The cutting angle was represented by θ, and it is the angle between cutting speed and zoy plane.

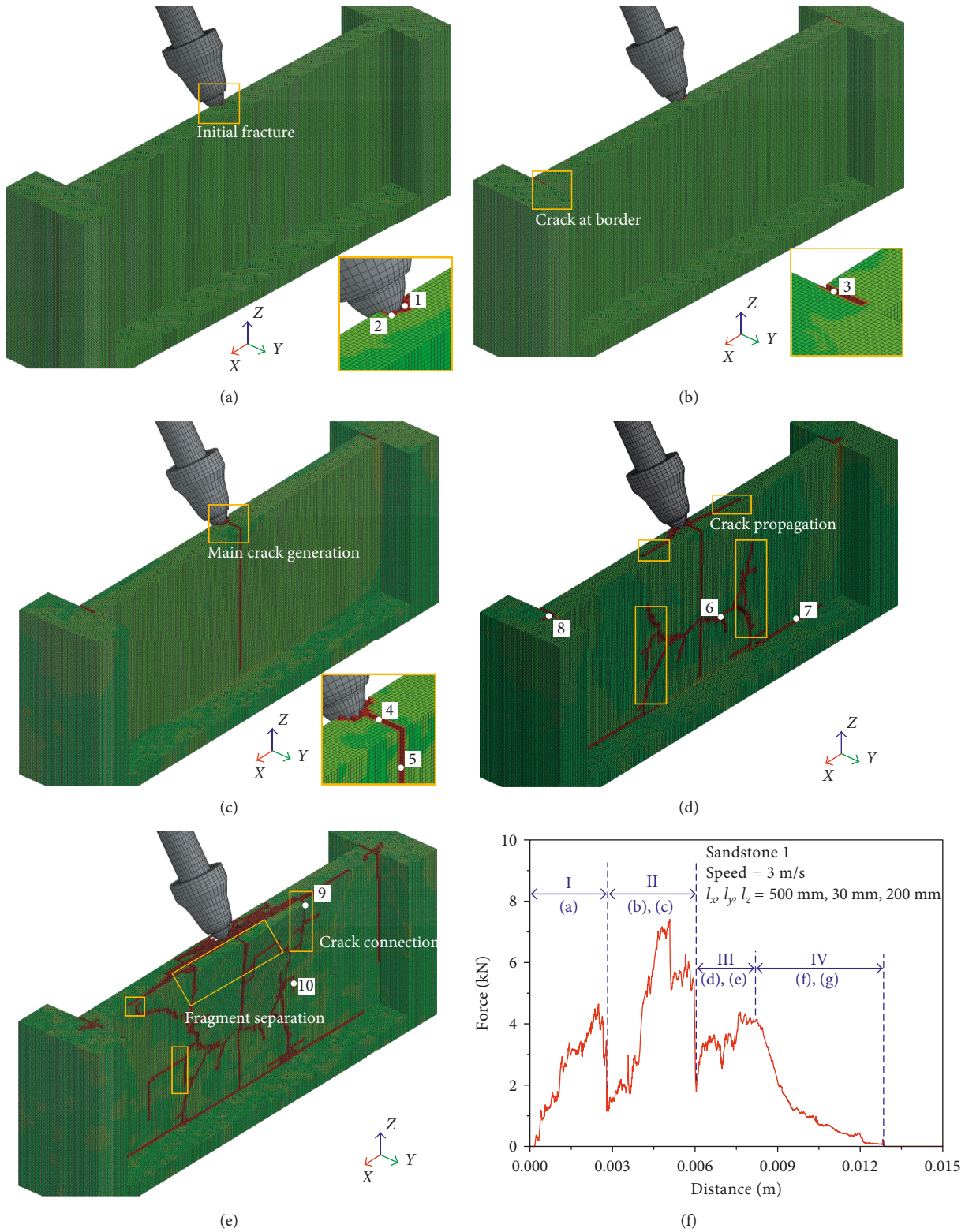

FIGURE 13: The rock cutting process for a cutting speed of 3 m/s, cutting position l_{xp}/l_x of 1/2, and width, thickness, and height of 500 mm, 30 mm, and 200 mm, respectively, for sandstone 1: (a) initial fracture, (b) crack at the border, (c) main crack generation, (d) crack propagation, (e) crack connection and fragment separation, and (f) variation in the cutting force.

The surface constraint conditions of the finite element model were applied as follows. Displacement boundary conditions were (a) all of the bottom nodes of the base rock were constrained in x-, y-, and z-direction, (b) nodes on the right and left surface of the base rock were constrained in x-direction, and (c) the conical pick was constrained in x- and

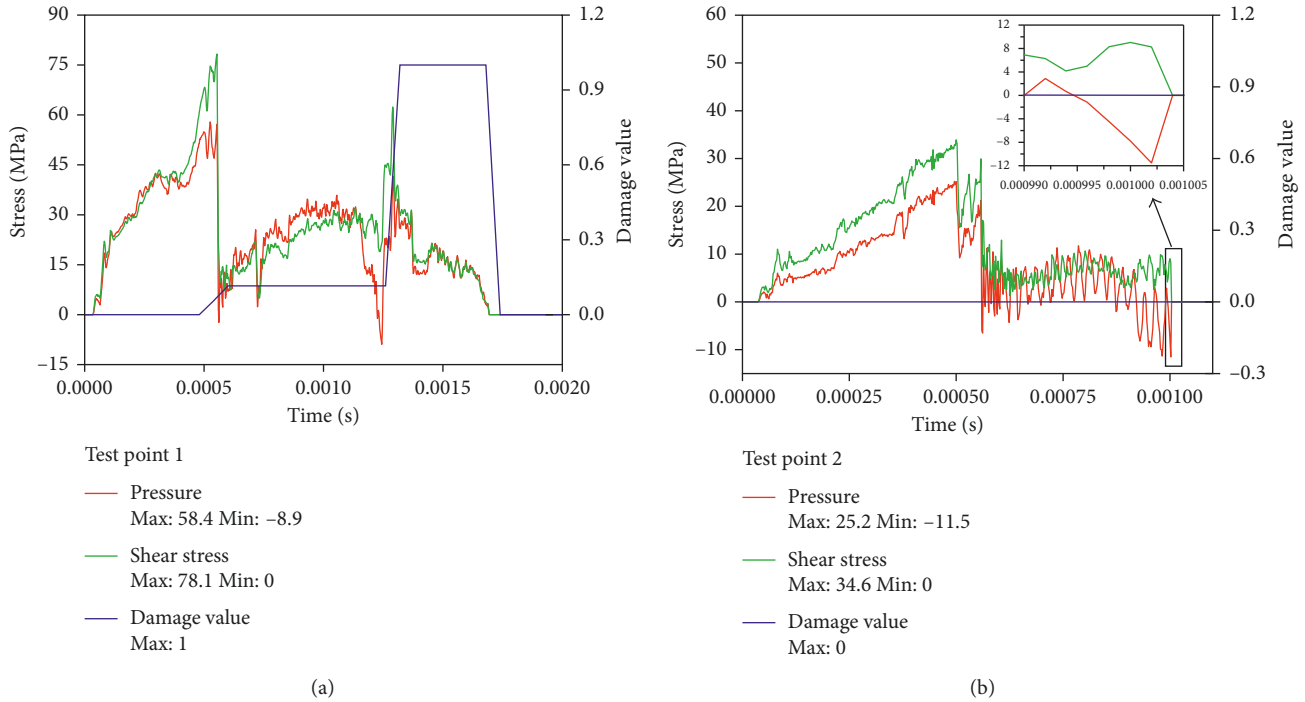

Figure 14: The variation in the stress with time: (a) test point 1 and (b) test point 2.

Table 4: The stress and damage values of the test points.

Test point		1	2	3	4	5	6	7	8	9	10
Pressure (MPa)	Maximum	58.4	25.2	0.6	1.4	0.3	4.9	16.3	4.2	0.7	13.4
	Minimum	−8.9	−11.5	−11.6	−11.6	−11.4	−11.5	−11.6	−11.5	−11.6	−11.6
Shear stress (MPa)	Maximum	78.1	34.6	10.0	11.1	14.1	12.3	13.9	21.1	16.7	15.3
Damage	Maximum	1	0	0	0	0	0	0	0	0	0

z-direction. In order to avoid the influence of the stress wave, nonreflecting boundary was applied to the entire surface.

3.4. Performance Check of Numerical Model. The experimental simulation and numerical simulation were carried out with the same cutting parameters for granite. The cutting angle is 0°, and cutting position $l_{xp}/l_x = 1/2$. The thickness of granite was 20 mm. The experimental result and numerical result with l_x of 400 mm and l_y of 120 mm for granite are shown in Figure 11. The crack propagation and cutting results are similar between experimental and numerical results. Fracture appeared at junctional position of free side and clamped side and at the middle of the free surface. It was consistent with the theoretical results.

The variation of the cutting force is shown in Figure 12. It is clear that the regulation of curves is similar between experimental and numerical results. The peak cutting force obtained from numerical simulation and experiment are very similar; therefore, the numerical method is available.

4. Numerical Results and Discussion

The cutting forces were obtained from numerical and experimental methods, but there is no comparison with the cutting force obtained from traditional rock cutting. The advantage of the rock plate cutting has not been shown. The experiment of the traditional rock cutting had been carried out by a linear cutting machine [8]. The mechanical properties of the rock in the experiment are shown in Table 3. With these parameters, the numerical simulations were carried out. The other numerical parameters were the same as given in Table 2.

4.1. The Rock Plate Cutting Process and Variation of Cutting Force. The numerical results of rock cutting process for a cutting speed of 3 m/s, cutting angle of 0°, and cutting position l_{xp}/l_x of 1/2 for sandstone 1 are shown in Figure 13. With the movement of the conical pick, a cutting force was exerted on the rock plate, and then the fragment separated from the rock plate. As shown in Figure 13(a), the rock plate was crushed only at the position around the conical pick. The variation in cutting force is shown in Figure 13(f), stage I. With the increasing cutting distance of conical pick, the cutting force increased. With the element failure and deleted from the rock plate, the cutting force decreased rapidly. As shown in Figure 13(b), the rock plates fracture not only around the cutting pick, but also at the place of the border between rock plate and base rock. With the increasing

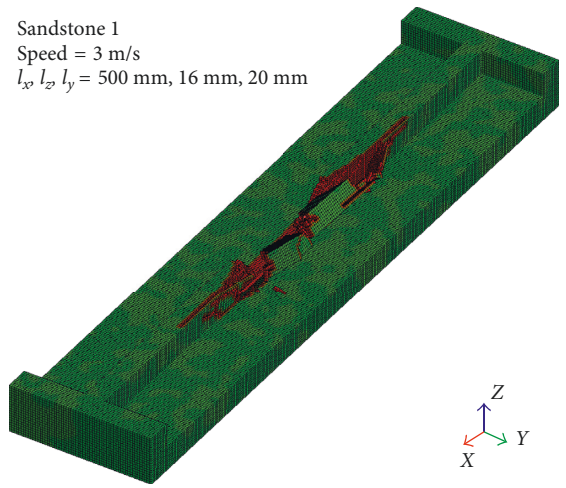

(a)

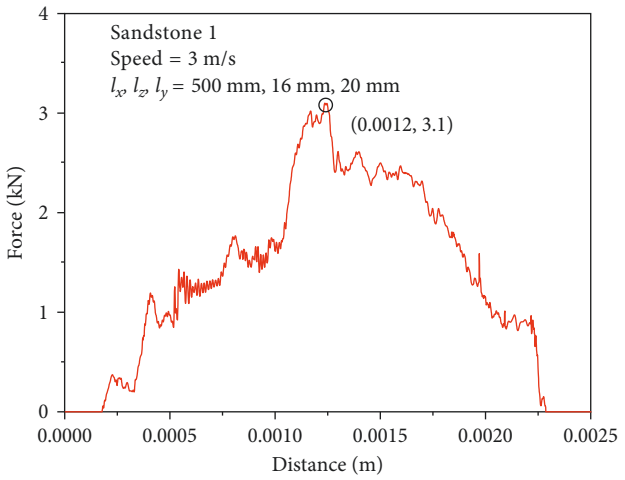

(b)

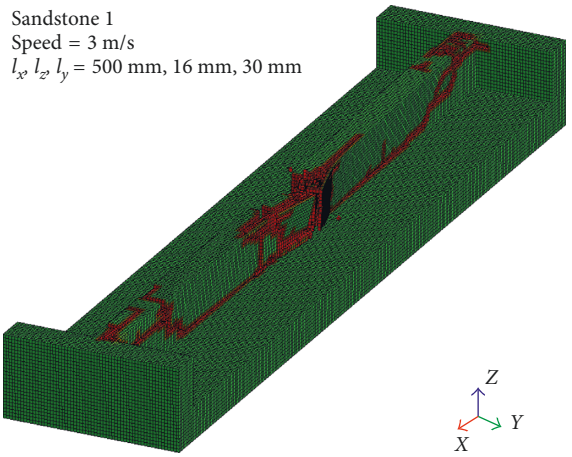

(c)

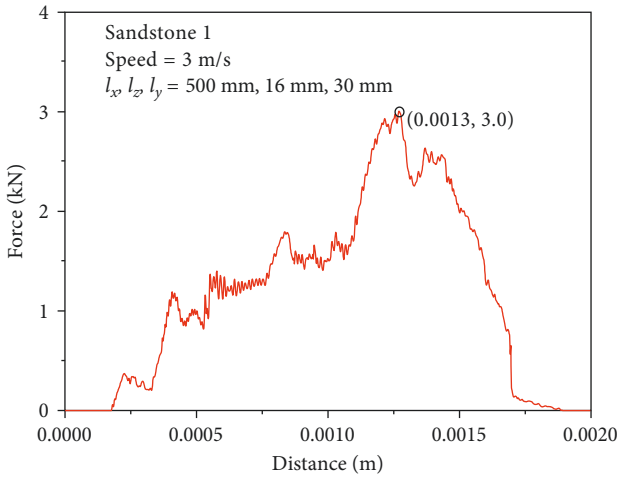

(d)

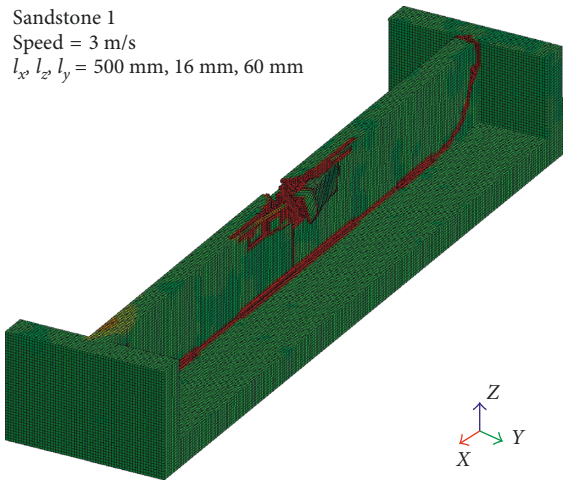

(e)

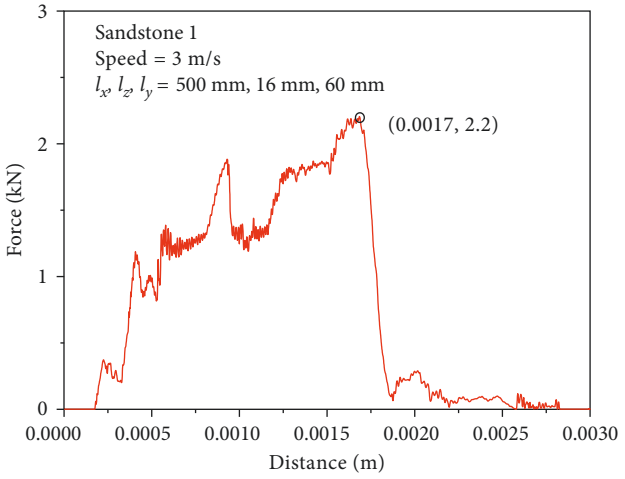

(f)

Figure 15: Continued.

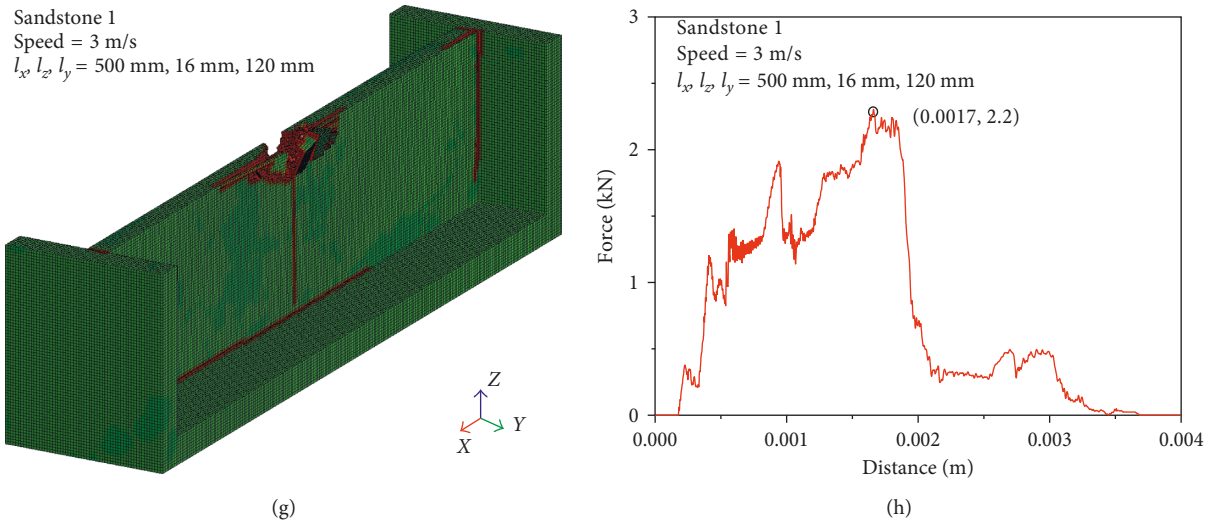

FIGURE 15: The cutting results with l_x of 500 mm, l_y of 16 mm, and cutting speed of 3 m/s for sandstone 1: (a), (c), (e), and (g) are l_z of 20 mm, 30 mm, 60 mm, and 120 mm, respectively, and (b), (d), (f), and (h) are the corresponding cutting forces.

cutting force as shown in Figure 13(f), stage II, the elements at the border were subjected to tensile stress and failure because of the elastic deformation. Therefore, the crack first appeared at the border. As shown in Figure 13(c), a main crack extended from the cutting position in the middle of the rock plate. This can be explained by the factor that the middle of the rock plate bore greater tensile stress and was easier to failure. In this cutting process, the cutting force reached to the maximum value, as shown in Figure 13(f). Subsequently, some tiny cracks propagated from the main crack as shown in Figures 13(d); with the movement of the pick, the cracks propagated rapidly and irregularly on the surface and the inside of the rock plate. The rock plate border generated more crush regions, and the crack extended to the base rock. The cutting force in this process showed an increasing trend as shown in Figure 13(f), stage III. As shown in Figure 13(e), with increasing cutting distance, the cracks connected to each other in the surface and inside of the rock plate, and then the fragment with random size and shape was separated from the rock plate. The cutting force decreased in this process as shown in stage IV. Figure 13(e) also shows that considerable cracks remain on the rock plate as the results of rock cutting. These results provided the foundation for reducing cutting force when the rock plate is cut again.

4.2. The Failure Mode of the Rock. Failure mode of the rock plate is very important for researching the cutting force and fracture process. As shown in Figure 14, ten failure elements in different places were selected to research the failure mode in the saw blade-conical pick cutting method. Three failure modes may occur in the rock cutting process: tensile, compressive, and shear failure. The tensile stress value reaching to 11.6 MPa indicates tensile failure, while the damage value of the element reaching to 1 indicates the compressive failure, otherwise the element shear failure. The three failure modes do not occur simultaneously. The positive value of the pressure indicates the rock bore compressive stress. The negative value of the pressure indicates the rock bear tensile stress. As shown in Figure 14(a), the test point 1 bore the minimum pressure of −8.9 MPa, less than limited tensile strength of −11.6 MPa, while the damage value of test point 1 reached to 1. It indicated that test point 1 experienced compressive damage failure. As shown in Figure 14(b), the damage value of test point 2 was zero, so the element failure was not caused by compressive stress. The minimum pressure of −11.5 MPa indicated that the failure mode of test point 2 was tensile failure. The failure pressure was slightly greater than −11.6 MPa due to the data sampling frequency. Among the ten test points, nine of them experienced tensile failure and one experienced compressive failure as shown in Table 4. It can be concluded that the main failure mode of rock is tensile failure, and a few elements experienced compressive failure at the position around the conical pick. The ultimate tensile strength is the main dominant property for the rock failure during rock plate cutting process.

4.3. The Height of the Rock Plate Influenced on the Cutting Performance. The cutting results for the simulation that were carried out at a cutting speed of 3 m/s, l_x of 500 mm, l_y of 16 mm, and l_z of 20 mm, 30 mm, 60 mm, and 120 mm with sandstone 1 are shown in Figure 15. During the cutting process, the fragments separated from rock plate with random morphology and size and cracks propagated irregularly. It was easier to generate fragments near the pick-rock interaction region. The rock fracture from the bottom border with the lower l_z is shown in Figure 15(a). At the end of the cutting process, there were no cracks remained on the rock plate. With the increasing l_z, more cracks generated on the rock plate as shown in Figures 15(c) and 15(e) besides the fragment separation. The cracks basically were close to the arc. It agreed with experimental results. When l_z increased to

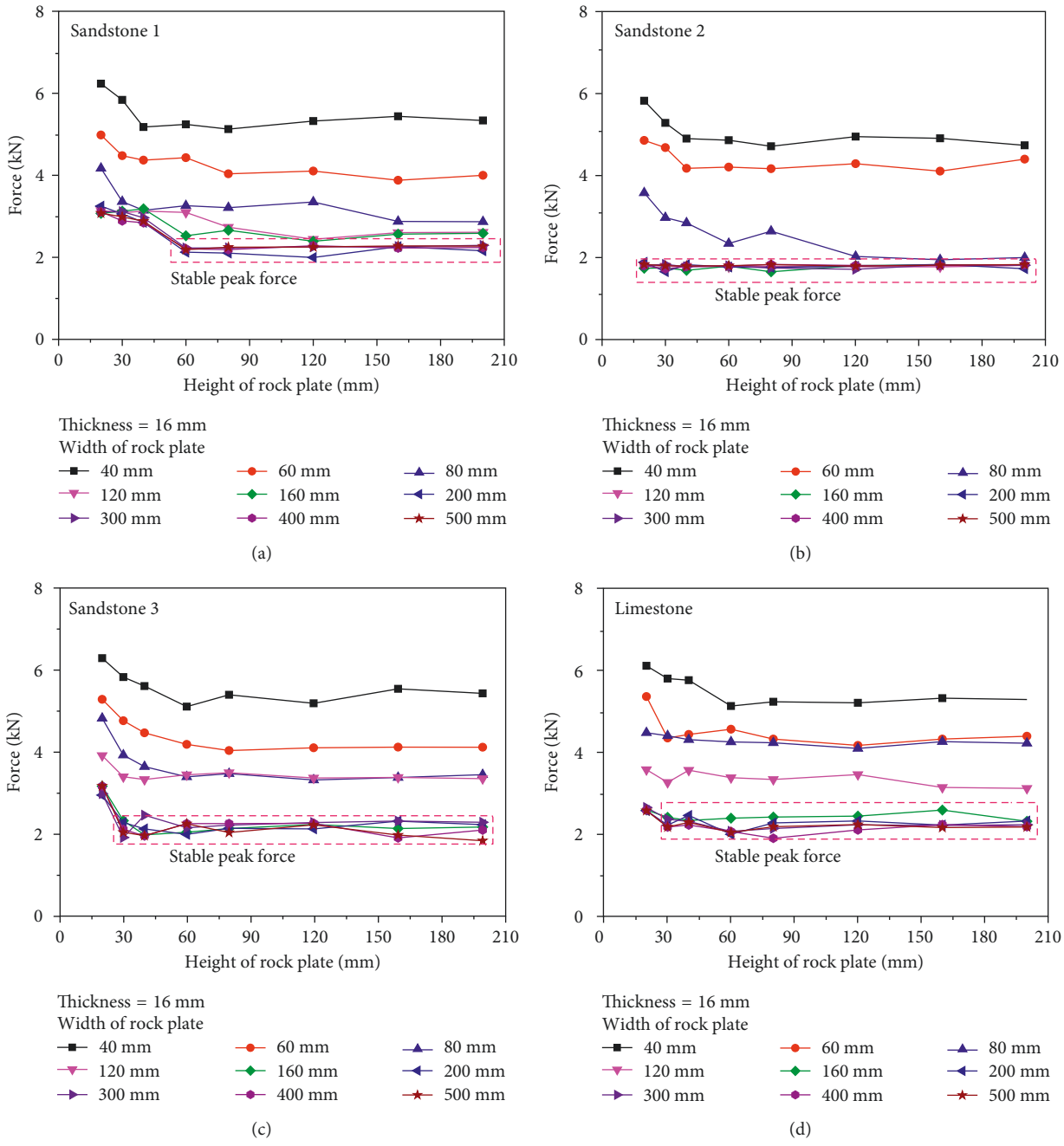

Figure 16: The variation in peak cutting force with height of rock plate for different rock properties: (a) sandstone 1, (b) sandstone 2, (c) sandstone 3, and (d) limestone.

Table 5: The minimum height and width corresponding to stable peak force for thickness of 16 mm.

Rock name	Sandstone 1	Sandstone 2	Sandstone 3	Limestone
Height (mm)	60	20	30	30
Width (mm)	200	120	160	200
Stable peak force (kN)	2.3	1.7	2.0	2.2

120 mm, all of the cracks were generated on the edge of the rock plate. Therefore, the larger l_z was more favorable for next step rock cutting because there were more cracks. This can reduce cutting force effectively. The peak cutting forces for l_z of 20 mm, 30 mm, 60 mm, and 120 mm were 3.1 kN, 3.0 kN, 2.2 kN, and 2.2 kN as shown in Figures 15(b), 15(d), 15(f), and 15(h), respectively. It is clear that the peak cutting force decreased with the increasing l_z and finally tended to be stable. The corresponding cutting distances to the peak cutting forces were 0.0012 m, 0.0013 m, 0.0017 m, and

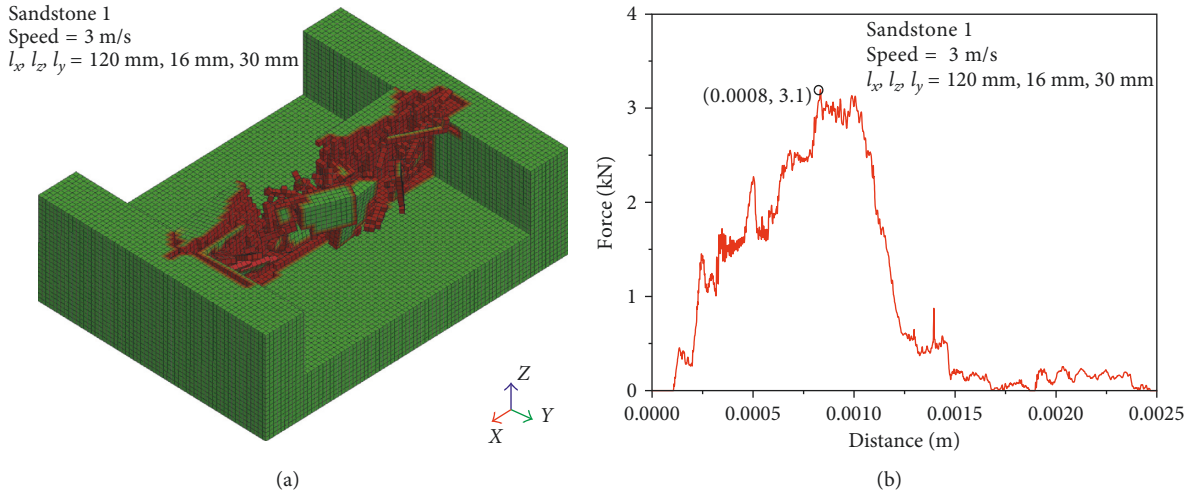

FIGURE 17: The cutting results with l_x of 120 mm, l_y of 16 mm, l_z of 30 mm, and cutting speed of 3 m/s for sandstone 1: (a) fracture results and (b) the variation of cutting force with cutting distance.

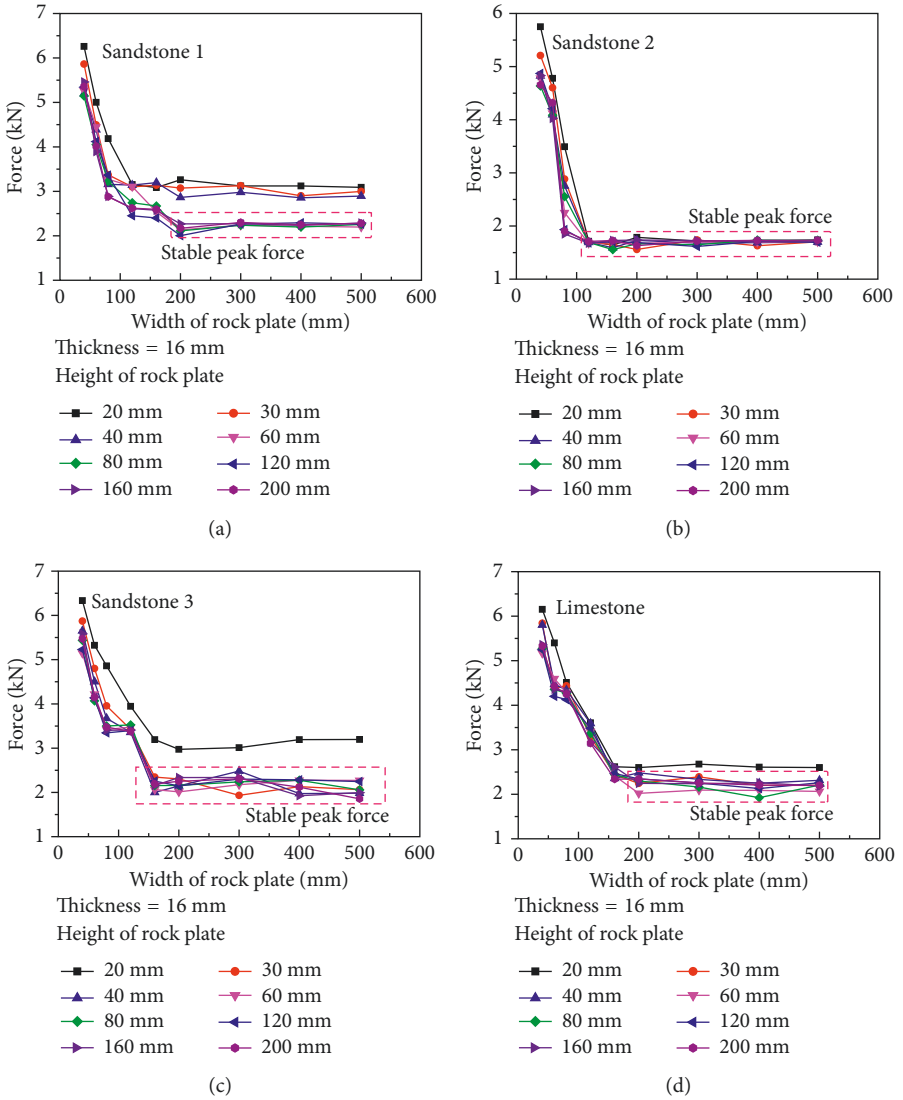

FIGURE 18: The variation in peak cutting force with width of rock plate for different rock properties: (a) sandstone 1, (b) sandstone 2, (c) sandstone 3, and (d) limestone.

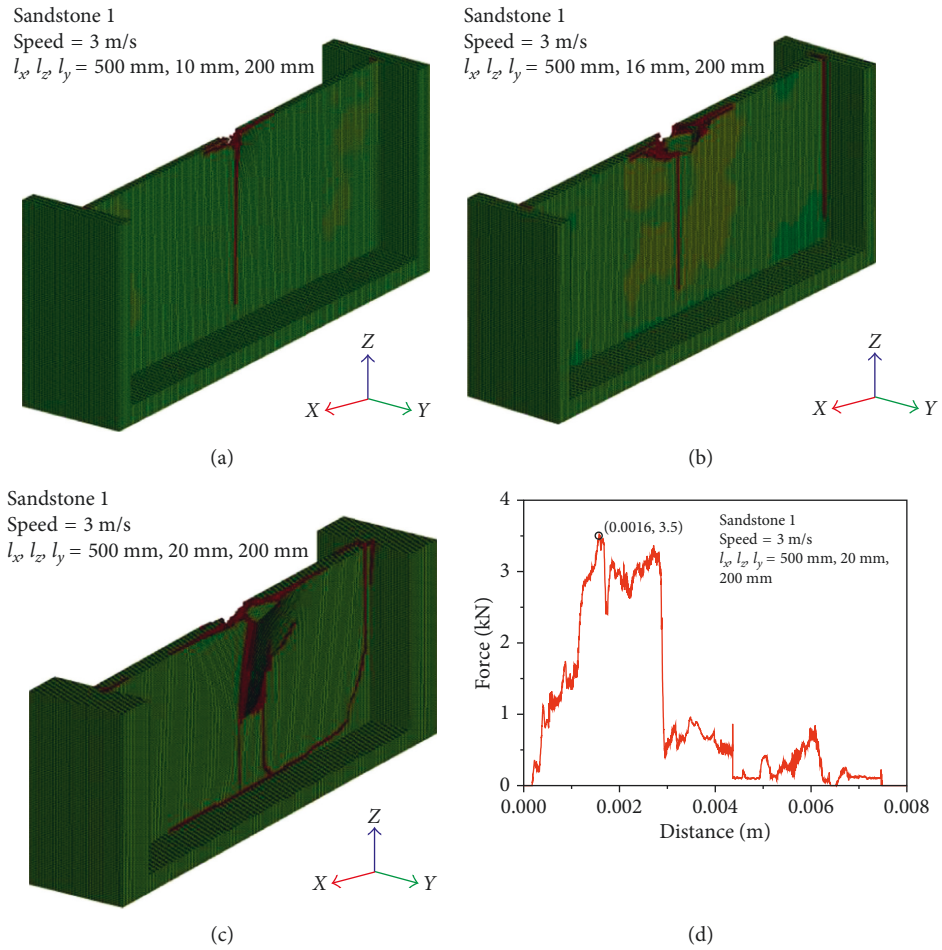

Figure 19: The cutting results of the rock with a cutting speed of 3 m/s, l_x of 500 mm, and l_z of 200 mm: (a) l_y of 10 mm, (b) l_y of 16 mm, (c) l_y of 20 mm, and (d) the variation of cutting force.

0.0017 m. It increased with the increasing l_z and finally became stationary. It also can be seen that the variation of cutting force was similar before peak force generated when compared with Figures 15(b), 15(d), 15(f), and 15(h), while after peak force, the variation of cutting force was significantly different. The cutting force decreased rapidly with the higher l_z and decreased slowly with the lower l_z.

The relationships between the peak cutting force and height of rock plate for different rock properties are shown in Figure 16. The peak force decreased with increasing height of the plate. However, when the height increased to a certain value, the peak cutting force varied nonsignificantly. It also indicated that when both the height and the thickness of rock plate increased to a certain value, the peak force is stable for the certain thickness of plate. The minimum value of the peak force for a certain thickness of plate with various height and width was named as "stable peak force." With the thickness of 16 mm, the minimum height and width corresponded to the stable peak force were 60 mm and 200 mm, as shown in Table 5. It means if the height is more than 60 mm and width is more than 200 mm, the peak cutting force should be stable peak force.

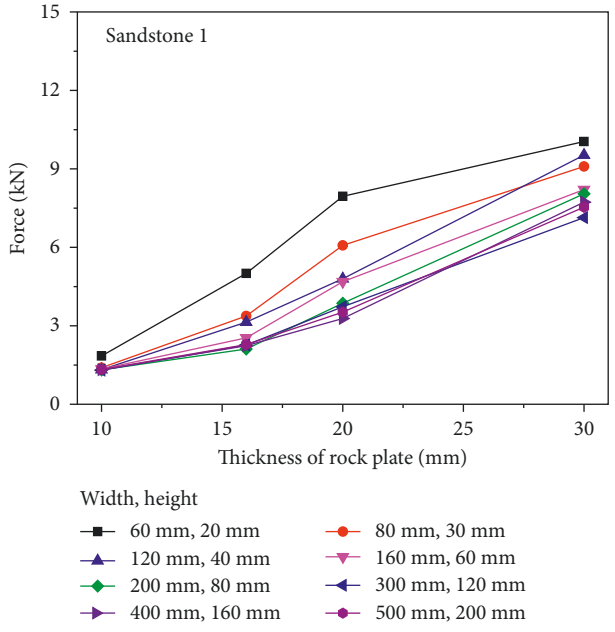

Figure 20: The variation in peak force with thickness of rock plate.

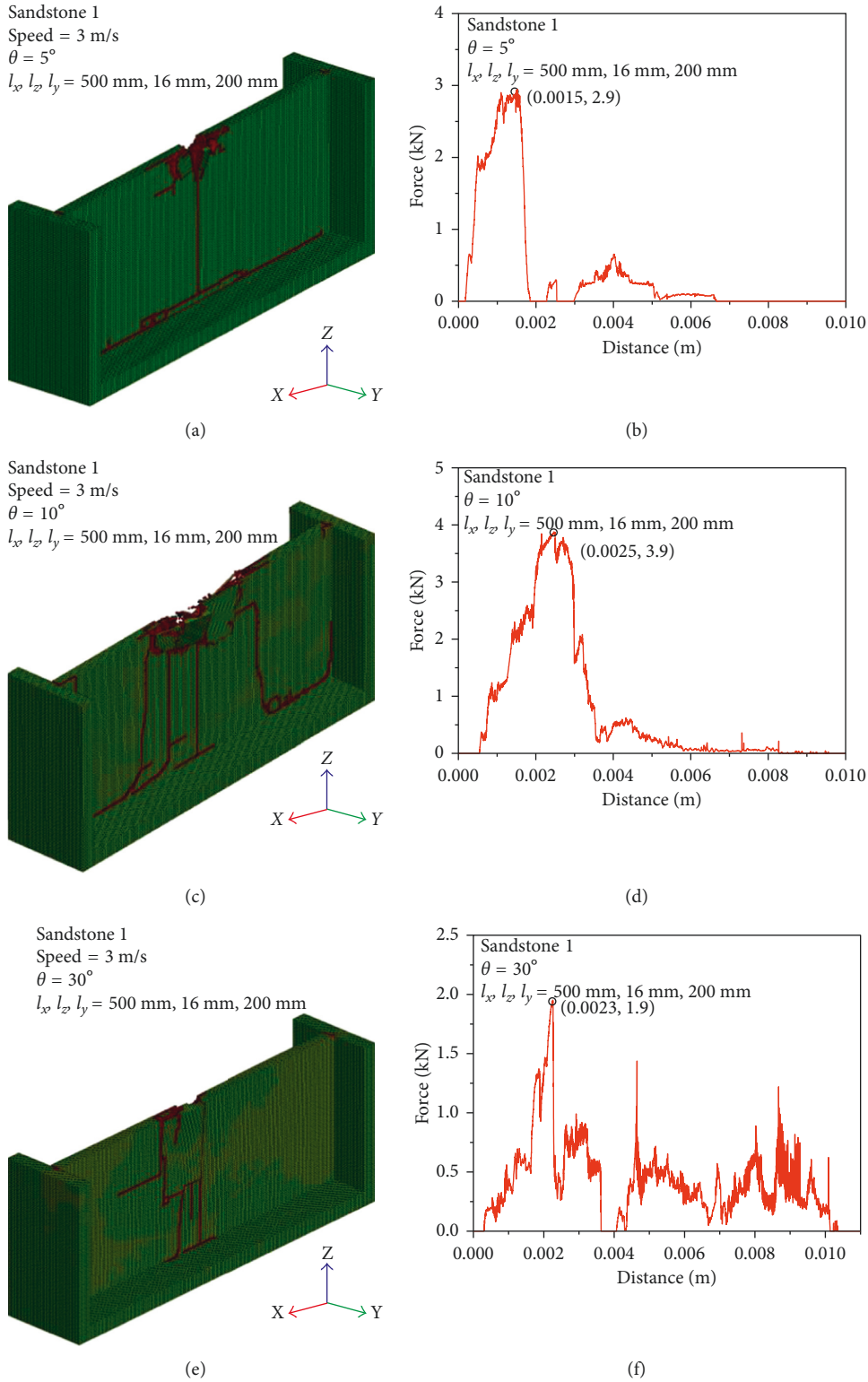

FIGURE 21: The cutting results with l_x of 500 mm, l_y of 16 mm, and l_z of 200 mm for sandstone 1: (a), (c), and (e) are cutting results for θ of 5°, 10°, and 30°, respectively, and (b), (d), and (f) are the variation in cutting force for θ of 5°, 10°, and 30°, respectively.

4.4. The Width of the Rock Plate Influenced on the Cutting Performance. Almost whole rock plate was crushed as shown in Figure 17(a) with l_x of 120 mm, while in Figure 15(c), part of rock plate was broken with l_x of 500 mm and the fracture region was bigger. It is indicated that l_x influenced the fracture region of plate when l_z and l_y were invariant. In detail, the fracture region increased with increasing l_x. However, when l_x increases to a certain value, the fracture

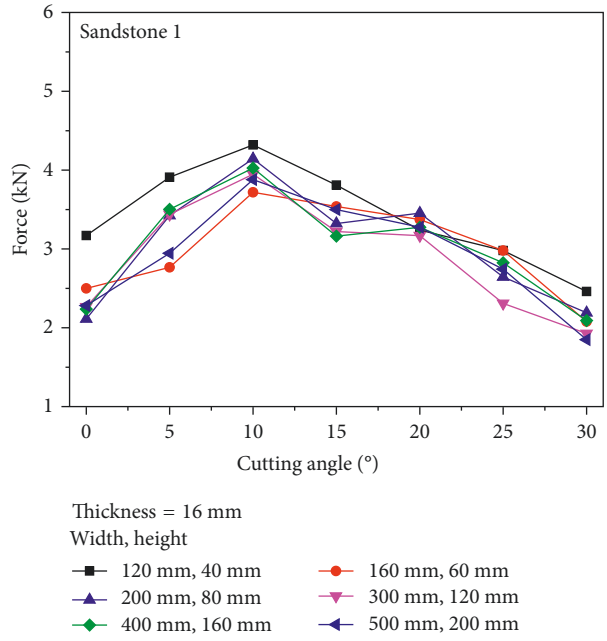

FIGURE 22: The variation in the peak force with cutting angle of θ.

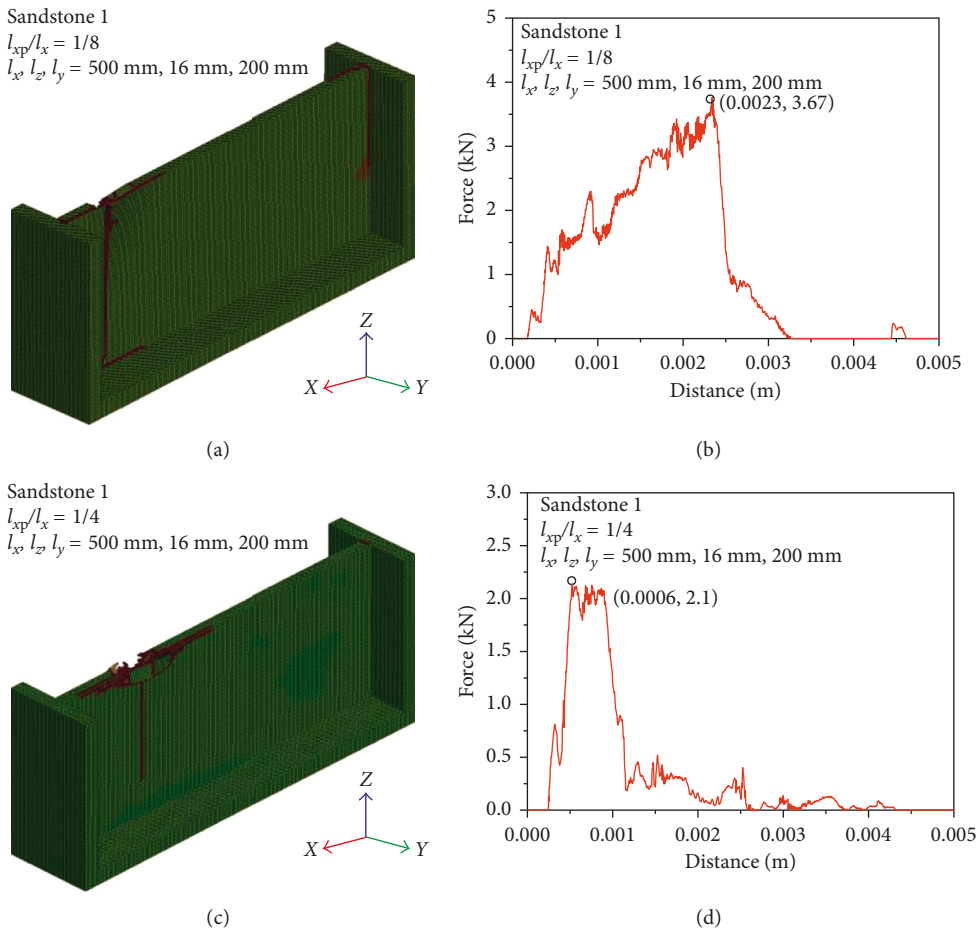

FIGURE 23: The cutting results with l_x of 500 mm, l_y of 16 mm, and l_z of 200 mm for sandstone 1: (a, c) the cutting results for l_{xp}/l_x of 1/8 and 1/4, and (b, d) the variation in cutting force with cutting distance for l_{xp}/l_x of 1/8 and 1/4.

area no longer increases. At the cutting distance of 0.0008 m, the cutting force reached to the maximum value of 3.1 kN as shown in Figure 17(b) and larger than 3.0 kN shown in Figure 15(c). So, the cutting force decreased with the increasing l_x. The cutting distance corresponding to the peak cutting force was increased with the increasing l_x.

The peak force varied significantly with the lower width of plate as shown in Figure 18. When compared with Figure 16, the peak force had a sharper decrease with decreasing width. Specifically, width had a greater influence on peak force than height. It can be attributed to constraint condition of the rock plate. In detail, the constrained left side and right side lead to the rock plate harder to deform in the width direction. In the height direction, only the bottom was constrained, and therefore, it is easy to deform and crush. The minimum height and width corresponding to stable peak force were obtained from Figure 18 and were the same as given in Table 5.

4.5. The Thickness of the Rock Plate Influenced on the Cutting Performance. The cutting results with different thickness of 10 mm, 16 mm, 20 mm, and 30 mm as shown in Figures 19(a) and 19(c) and 13(e) were compared. There were little fragments generated in the cutting process with the thickness of 10 mm as shown in Figure 19(a). As for crack, only the main crack generated. When the thickness was increased to 16 mm, both middle and border obtained cracks as shown in Figure 19(b). When the thickness is of about 20 mm and 30 mm, cracks appeared on the rock plate randomly and the quantity increased rapidly. Accordingly, the quantity and size of cracks and fragments increased with increasing thickness. The peak force obtained in thickness of 20 mm was 3.5 kN, while that in the thickness of 30 mm was 7.4 kN. The higher the thickness, the higher the cutting force.

To study the thickness influenced on the peak cutting force, 8 group numerical results were extracted for analyzing the regularities. The thickness of the rock plate had a significant influence on peak cutting force as shown in Figure 20. All of the minimum peak forces were obtained in the thickness 10 mm, while all of the maximum peak forces were obtained in the thickness of 30 mm. The peak force increased with increasing thickness of rock plate significantly. It was because the bending strength of the plate increased with the thickness of the rock, and the rock plate with large bending strength would bring out greater resistance.

4.6. The Cutting Angle Influenced on the Cutting Performance. By comparing the cutting results shown in Figures 19(b), 21(a), and 21(c) with θ of 0°, 5°, and 10°, the cutting results with θ of 0° obtained the fewest cracks. In contrary, θ of 10° obtained the most cracks. It is indicated that the quantity of the cracks had a strong association with θ. The quantity of the cracks and fragments increased with increasing θ. However, θ of 30° obtained fewer cracks when compared with θ of 5° and 10°. It is interesting that cracks obtained only at one side of the rock plate as shown in Figure 21(e) with θ of 30°. So, it can be concluded that too higher values of θ reduced the crush region of the rock plate. The peak force

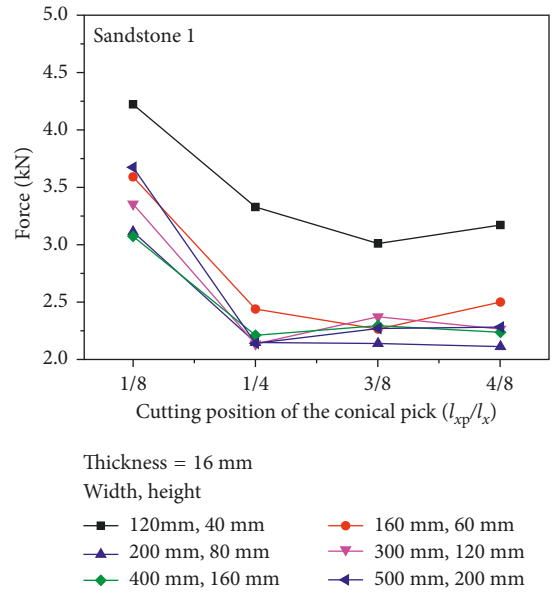

Figure 24: The variation in the peak force with cutting position of l_{xp}/l_x.

obtained in θ of 0° was 2.2 kN. It is lower than 2.9 kN and 3.9 kN that were obtained in θ of 5° and 10° as shown in Figures 21(b) and 21(d). However, the fewest peak force with 1.9 kN was obtained in θ of 30° as shown in Figure 21(f). The wave form is also significantly different from Figures 21(b) and 21(d). There are three peak forces in the cutting process for θ of 30°, and the frequency of the cutting force increased. Meanwhile, the cutting distance obviously increased with the increasing cutting angel.

The variation in peak force with cutting angle is shown in Figure 22. The influence of cutting angle on peak force is significant. The curve shows that peak force increased first and then decreased with the increasing cutting angle. All of the maximum peak force obtained at cutting angle of 10°, while all of the minimum peak force obtained at cutting angle of 30°.

4.7. The Cutting Position Influenced on the Cutting Performance. Cutting position (l_{xp}/l_x) is a key factor influence on peak cutting force, and l_{xp} is as shown in Figure 10. The previous studies were all carried out at l_{xp}/l_x of 1/2. To study l_{xp}/l_x influence on the peak force, l_{xp}/l_x of 3/8, 1/4, and 1/8 were also carried out for simulation. Crack and fragment vary nonsignificantly with the decrease of l_{xp}/l_x as shown in Figures 19(b), 23(a), and 23(c). In contrary, by comparing Figures 19(b) and 19(d), the peak forces were significantly different. With l_{xp}/l_x of 1/8 and 1/4, 3.67 kN and 2.1 kN of the peak forces were obtained.

As shown in Figure 24, the peak force decreased significantly with l_{xp}/l_x of 1/8 increase to 1/4. However, the cutting force was stable with l_{xp}/l_x increase from 1/4 to 1/2. As a conclusion, peak force decreased with increasing l_{xp}/l_x and then became stable. The cutting position near the border between rock plate and base rock should be avoided during the cutting process.

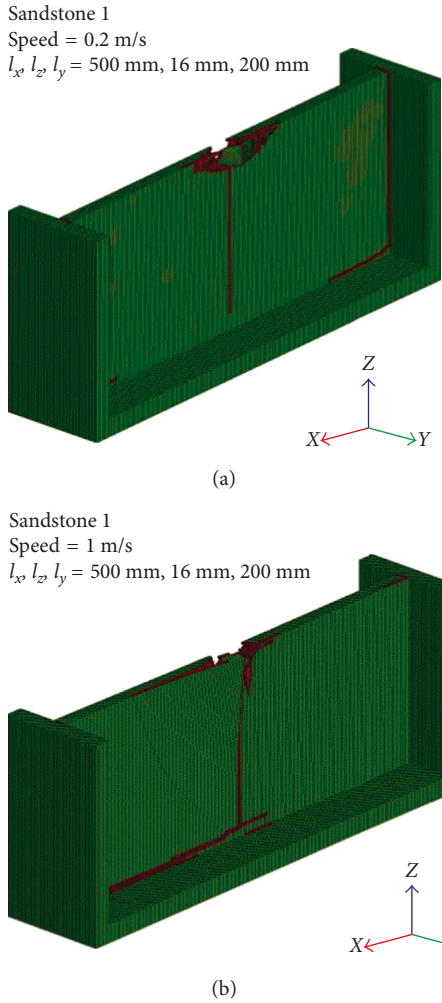

Figure 25: The cutting results with l_x of 500 mm, l_y of 16 mm, and l_z of 200 mm for sandstone 1: (a) the cutting results for cutting speed of 0.2 m/s and (b) the cutting results for cutting speed of 1 m/s.

4.8. The Cutting Speed Influenced on the Cutting Performance. It is indicated that cutting speed has nonsignificant influence on the cutting performance by comparing cutting results with cutting speed of 3 m/s as shown in Figure 19(b), 0.2 m/s as shown in Figure 25(a), and 1 m/s as shown in Figure 25(b). Cracks obtained in the three cutting speeds were very similar to each other, although there was a little difference (Figure 25).

The cutting speed had no obvious influence on cutting force as shown in Figure 26. This result is same to the traditional rock cutting that, in the lower cutting speed, the cutting force varies nonsignificantly [23]. Therefore, it was meaningless to research the cutting speed influence on cutting performance and cutting peak force.

4.9. Regression Analysis between Peak Force and Variables. The strong correlation was obtained between peak force and the cutting variables as shown in Figure 23. The exponential relationships exist between peak cutting force and height, width, and thickness of rock plate as shown

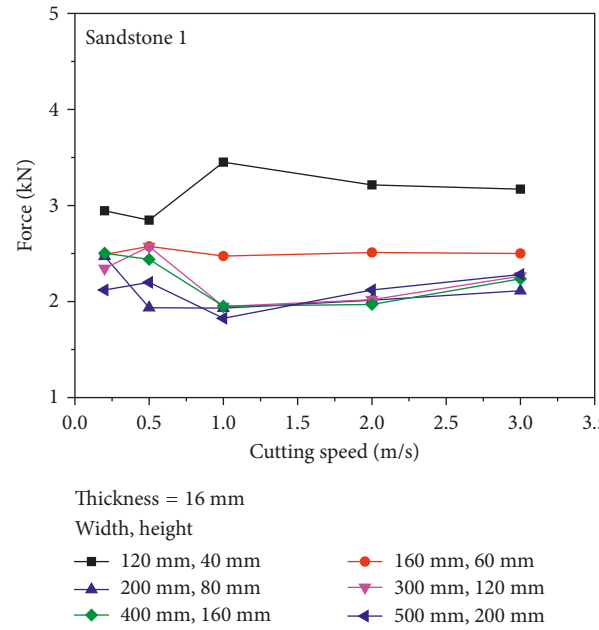

Figure 26: The variation in the peak force with cutting speed.

in Figures 27(a) and 27(c). The correlation coefficients of 0.8620, 0.8148, 0.9848, 0.9758, 0.9997, and 0.9768 showed strong agreement between the cutting variables and peak force. A binomial relationship exists between peak force and cutting angle, and an exponential relationship exists between peak force and cutting position of l_{xp}/l_x as shown in Figures 27(d) and 27(e) The coefficients of 0.669, 0.9153, 0.9786, and 0.9763 indicate that the analysis results are satisfied.

The confidence level is very important to evaluate the accuracy of regression analysis results. 0.95 is most frequently used confidence level [23]. At the confidence of 0.95, the regression results to predict the peak cutting force are shown in Table 6. The maximum and minimum P values are $4.8e^{-2}$ and $6.0e^{9}$, lower than 0.05, certifying that the regression analysis results are valid and reliable.

4.10. The Comparison between Rock Plate Cutting and Linear Rock Cutting. Since the new cutting method aim to decrease the cutting force, the comparison between rock plate cutting and classic linear rock cutting is necessary. The stable peak cutting force for sandstone 1, sandstone 2, sandstone 3, and limestone with thickness of 30 mm were 7.5 kN, 6.1 kN, 4.9 kN, and 5.6 kN, respectively. The peak cutting force that was obtained from linear rock cutting experiment was 48.7 kN. 28.1 kN, 15.9 kN, and 29.4 kN for sandstone 1, sandstone 2, sandstone 3, and limestone, respectively [7]. The comparison between rock plate cutting and linear rock cutting is shown in Figure 28. It was obvious that rock plate cutting force was significantly smaller than linear rock cutting.

5. Conclusion

In this research, a new rock cutting method was proposed. To predict the cutting performance and peak force of the

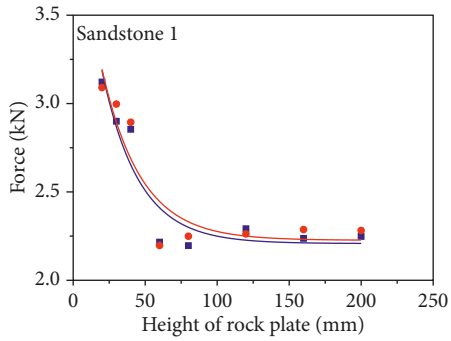

Thickness = 16 mm
Width
- 400 mm
  $y = 2.20972 + 2.15256\exp(-0.03941x)$, $R^2 = 0.86204$
- 500 mm
  $y = 2.22638 + 2.03257\exp(-0.03707x)$, $R^2 = 0.81477$

(a)

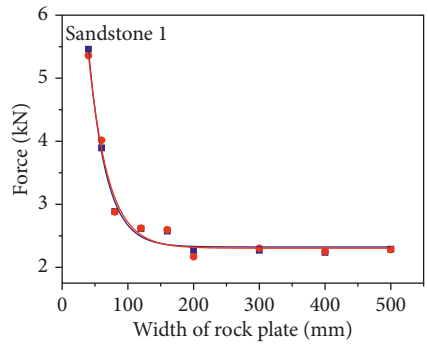

Thickness = 16 mm
Height
- 160 mm
  $y = 2.32392 + 13.7128\exp(-0.03684x)$, $R^2 = 0.98484$
- 200 mm
  $y = 2.30385 + 11.7590\exp(-0.03352x)$, $R^2 = 0.97576$

(b)

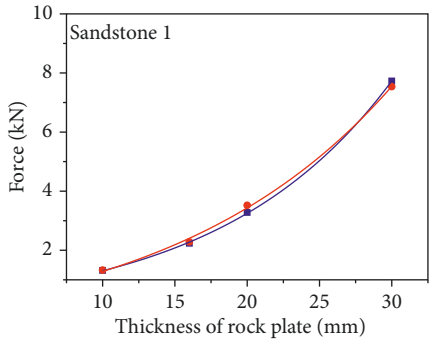

Width, height
- 400 mm, 160 mm
  $y = -0.19038 + 0.64984\exp(0.08336x)$, $R^2 = 0.9997$
- 500 mm, 200 mm
  $y = -1.07126 + 1.2321\exp(0.06483x)$, $R^2 = 0.996667$

(c)

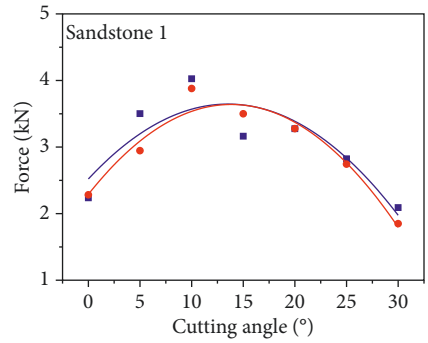

Thickness = 16 mm
Length, height
- 400 mm, 160 mm
  $y = 2.52079 + 0.16632x - 0.00615x^2$, $R^2 = 0.669180$
- 500 mm, 200 mm
  $y = 2.29038 + 0.19510x - 0.00705x^2$, $R^2 = 0.9153$

(d)

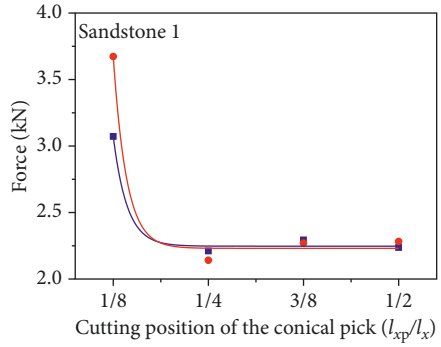

Thickness = 16 mm
Width, height
- 400 mm, 160 mm
  $y = 2.24707 + 790.52\exp(-54.92394x)$, $R^2 = 0.97858$
- 500 mm, 200 mm
  $y = 2.23067 + 1883.8\exp(-57.40125x)$, $R^2 = 0.97629$

(e)

Figure 27: The relationship between peak cutting force and cutting variables: (a) height of rock plate, (b) width of rock plate, (c) thickness of rock plate, (d) cutting angle, and (e) cutting position of l_{xp}/l_x.

Table 6: Regression results to predict peak force.

Variables	Cutting parameter	Regression equation	Correlation coefficient	F value	P value
F-l_z	l_x of 400 mm	$y = 2.20972 + 2.15256\exp(-0.03941x)$	0.86204	849	$4.7e^{-7}$
F-l_z	l_x of 500 mm	$y = 2.22638 + 2.03257\exp(-0.03707x)$	0.81477	632	$9.8e^{-7}$
F-l_x	l_y of 160 mm	$y = 2.32392 + 13.7128\exp(-0.03684x)$	0.98484	1645	$6.0e^{-9}$
F-l_x	l_y of 200 mm	$y = 2.30385 + 11.7590\exp(-0.03352x)$	0.97576	1044	$2.3e^{-8}$
F-l_y	l_x and l_z of 400 mm and 160 mm	$y = -0.19038 + 0.64984\exp(0.08336x)$	0.9997	10662	$6.9e^{-3}$
F-l_y	l_x and l_z of 500 mm and 200 mm	$y = -1.07126 + 1.2321\exp(0.06483x)$	0.97680	1022	$2.2e^{-2}$
F-θ	l_x and l_z of 400 mm and 160 mm	$y = 2.52079 + 0.16632x - 0.00615x^2$	0.669	7	$4.8e^{-2}$
F-θ	l_x and l_z of 500 mm and 200 mm	$y = 2.29038 + 0.19510x - 0.00705x^2$	0.9153	33	$3.2e^{-3}$
F-l_{xp}/l_x	l_x and l_z of 400 mm and 160 mm	$2.24707 + 790.52\exp(-54.92394x)$	0.97858	2235	$1.5e^{-2}$
F-l_{xp}/l_x	l_x and l_z of 500 mm and 200 mm	$2.23067 + 1883.8\exp(-57.40125x)$	0.97629	763	$2.5e^{-2}$

conical pick, numerical simulations were carried out. The feasibility of numerical method was verified by the experimental results. In the simulation, the compressive damage constitutive model was combined with erosion criteria for controlling the rock failure. The peak cutting force and cutting performance were studied with varying thickness, height, and width of the rock plate. The cutting angle, cutting speed, and cutting position of the conical pick influence on peak force were also researched.

(1) The numerical result agreed with the experiment results. It indicated that the numerical method is an effective method to study rock plate cutting.

(2) The cutting process of rock plate in the simulation was in good correspondence with the theoretical. Rock plate fractures at the intersection of free side and fixed sides, and the middle of the free side.

(3) The cracks obtained during the cutting process varied significantly with varying thickness, height, and width of rock plate. However, the cracks varied nonsignificantly with cutting speed and cutting position of the conical pick. With increasing cutting angle, cracks increased and then decreased.

(4) The peak force also varied significantly with varying thickness, height, and width of rock plate. With increasing width, height of rock plate, and the cutting positing of l_{xp}/l_x, the peak cutting force decreased and remained stable. Moreover, the peak cutting force increased with increasing thickness and increased and decreased with increasing cutting angle. And finally, the peak force varied nonsignificantly with varying cutting speed.

(5) The correlation coefficients obtained between peak force and cutting parameters were ideal, indicating a strong relationship between peak force and cutting parameters of rock plate and conical pick. The P values obtained at the confidence level of 0.95 were all lower than those of other confidence levels, indicating that the regression results are reliable.

Conflicts of Interest

The authors declare that there are no conflicts of interest regarding the publication of this paper.

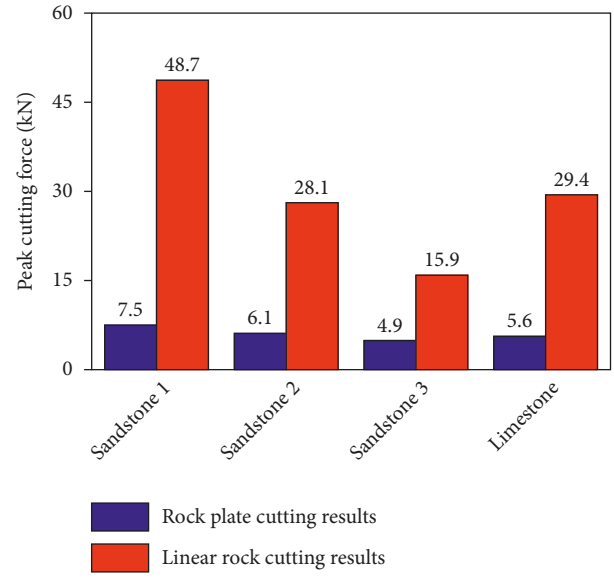

Figure 28: The comparison between numerical and experimental results.

Acknowledgments

This work was supported by projects of the National Natural Science Foundation of China (Grant no. 51674155) and the Natural Science Foundation of Shandong Province (Grant nos. ZR2016EEM02 and ZR2017MEE034) and by Special Funds for Cultivation of Taishan Scholars.

References

[1] I. Evans, "Line spacing of picks for effective cutting," *International Journal of Rock Mechanics and Mining Sciences and Geomechanics Abstracts*, vol. 9, no. 3, pp. 355–361, 1972.

[2] I. Evans, "Optimum line spacing for cutting picks," *Mining Engineer*, vol. 141, pp. 433-434, 1982.

[3] I. Evans, "A theory of the cutting force for point-attack picks," *Geotechnical and Geological Engineering*, vol. 2, no. 1, pp. 63–71, 1984.

[4] R. M. Goktan, "A suggested improvement on Evans' cutting theory for conical bits," in *Proceedings of the Fourth International Symposium on Mine Mechanization and Automation*, vol. 1, p. A4, Queensland, Australia, July 1997.

[5] F. F. Roxborough and Z. C. Liu, "Theoretical considerations on pick shape in rock and coal cutting," in *Proceedings of the Sixth Underground Operator's Conference*, pp. 189–193, Kalgoorlie, Australia, November 1995.

[6] Y. Nishimatsu, "The mechanics of the rock cutting," *International Journal of Rock Mechanics and Mining Sciences*, vol. 9, no. 2, pp. 261–71, 1972.

[7] N. Biligin, M. A. Demircin, H. Copur, C. Balci, H. Tuncdemir, and N. Akcin, "Dominant rock properties affecting the performance of conical picks and the comparison of some experimental and theoretical results," *International Journal of Rock Mechanics and Mining Sciences*, vol. 43, no. 1, pp. 139–156, 2006.

[8] K. Kel, N. A. Akcin, H. Tuncdemir, and N. Bilgin, "Cuttability characteristics of high strength rocks for roadheader selection in Zonguldak Coalfield," in *Proceedings of the 10th International Symposium on Mine Planning and Equipment Selection*, pp. 19–21, New Delhi, India, November 2001.

[9] X. H. Liu, S. Y. Liu, L. Li, and X. X Cui, "Experiment on conical pick cutting rock material assisted with front and rear water jet," *Advances in Materials Science and Engineering*, vol. 2015, no. 1, pp. 1–10, 2015.

[10] J. Huang, Y. Zhang, L. Zhu, and W. Ting, "Numerical simulation of rock cutting in deep mining conditions," *International Journal of Rock Mechanics and Mining Sciences*, vol. 84, pp. 80–86, 2016.

[11] X. Y. Li, Y. G. Lv, S. B. Jiang, and Q. L. Zeng, "Effects of spiral line for pick arrangement on boom type roadheader cutting load," *International Journal of Simulation Modelling (IJSIMM)*, vol. 15, no. 1, pp. 170–180, 2016.

[12] X. Li, B. Huang, G. Ma, and Q. Zeng, "Study on roadheader cutting load at different properties of coal and rock," *Scientific World Journal*, vol. 2013, Article ID 624512, 8 pages, 2013.

[13] H. X. Jiang, C. L. Du, S. Y. Liu, and Z. H. Liu, "Numerical analysis of rock cutting based on fracture mechanics," *Rock and Soil Mechanics*, vol. 34, no. 4, pp. 1179–1184, 2013.

[14] H. Huang, E. Detournay, and B. Bellier, "Discrete element modelling of rock cutting," *Rock Mechanics for Industry*, vol. 1, no. 1, pp. 123–130, 1999.

[15] S. T. Lei and P. Kaitkay, "Distinct element modeling of rock cutting under hydrostatic pressure," *Key Engineering Materials*, vol. 250, no. 1, pp. 110–117, 2003.

[16] D. L. Yang, J. P. Li, L. P. Wang, K. D. Gao, Y. H. Tang, and Y. X. Wang, "Experimental and theoretical design for decreasing wear in conical picks in rotation-drilling cutting process," *International Journal of Advanced Manufacturing Technology*, vol. 77, no. 9–12, pp. 1571–1579, 2015.

[17] S. P. Timoshenko and S. Woinowsky-Krieger, *Theory of Plates and Shells*, McGraw-Hill, New York, NY, USA, 2nd edition, 1959.

[18] S. P. Timoshenko and J. M. Gere, *Theory of Elastic Stability*, McGraw-Hill, New York, NY, USA, 2nd edition, 1961.

[19] J. Jiang, P. Zhang, and L. Nie, "Fracturing and dynamic response of high and thick stratas of hard rocks," *Chinese Journal of Rock Mechanics and Engineering*, vol. 33, no. 7, pp. 1366–1374, 2014.

[20] J. O. Hallquist, *LS-DYNA Theory Manual*, vol. 3, pp. 25–31, Livermore Software Technology Corporation, Livermore, CA, USA, 2006.

[21] F. Zhang and E. Li, "A computational model for concrete subjected to large strains, high strain rates, and high pressures," *Explosion and Shock Waves*, vol. 22, no. 3, pp. 198–202, 2002.

[22] O. Su and N. A. Akcin, "Numerical simulation of rock cutting using the discrete element method," *International Journal of Rock Mechanics and Mining Sciences*, vol. 48, no. 3, pp. 434–442, 2011.

[23] Z. G. Lu, L. R. Wan, Q. L. Zeng, X. Zhang, and K. D. Gao, "Numerical simulation of fragment separation during rock cutting using a 3D dynamic finite element analysis code," *Advances in Materials Science and Engineering*, vol. 2017, Article ID 3024918, 17 pages, 2017.